

Round and pleated blisters: interface delamination in thin film deposition

Wenxiang Wang, Shengyao Chen, Jiacong Cao, Xiaoding Wei & Zhaohe Dai

To cite this article: Wenxiang Wang, Shengyao Chen, Jiacong Cao, Xiaoding Wei & Zhaohe Dai (17 Apr 2025): Round and pleated blisters: interface delamination in thin film deposition, International Journal of Smart and Nano Materials, DOI: [10.1080/19475411.2025.2493663](https://doi.org/10.1080/19475411.2025.2493663)

To link to this article: <https://doi.org/10.1080/19475411.2025.2493663>



© 2025 The Author(s). Published by Informa UK Limited, trading as Taylor & Francis Group.



Published online: 17 Apr 2025.



Submit your article to this journal [↗](#)



View related articles [↗](#)



View Crossmark data [↗](#)

Round and pleated blisters: interface delamination in thin film deposition

Wenxiang Wang^a, Shengyao Chen^b, Jiacong Cao^a, Xiaoding Wei^a and Zhaohe Dai^a

^aDepartment of Mechanics and Engineering Science, State Key Laboratory for Turbulence and Complex Systems, College of Engineering, Peking University, Beijing, China; ^bCAS Key Laboratory of Nanosystem and Hierarchical Fabrication, Nanofabrication Laboratory, CAS Center for Excellence in Nanoscience, National Center for Nanoscience and Technology, Beijing, China

ABSTRACT



Electron beam deposition is widely used in microelectronics manufacturing due to its ability to fabricate high-purity thin films at elevated rates. However, the formation of blisters during this process – resulting from delamination between the film and substrate – can compromise film integrity and adversely affect device performance. This study investigates the mechanisms behind blister formation during the deposition of gold/titanium (Au/Ti) films on SiO₂/Si substrates with a polymethyl methacrylate (PMMA) layer, a common configuration in electronics. Two distinct types of blisters are identified: round blisters and pleated blisters. Elemental analysis and in situ heating experiments revealed that round blisters originate from delamination at the Au-Ti-PMMA/SiO₂ interface, while pleated blisters result from delamination between the Au-Ti film and the PMMA layer. We provide a mechanics model that can quantify the energy required to delaminate the film-substrate interface and the strain within the blister regions. The results offer valuable perspectives on both the fabrication of thin films and the potential application of strain engineering, where controlled blistering may enhance the functional performance of thin films for use in advanced microelectronics.

ARTICLE HISTORY

Received 15 February 2025
Accepted 11 April 2025

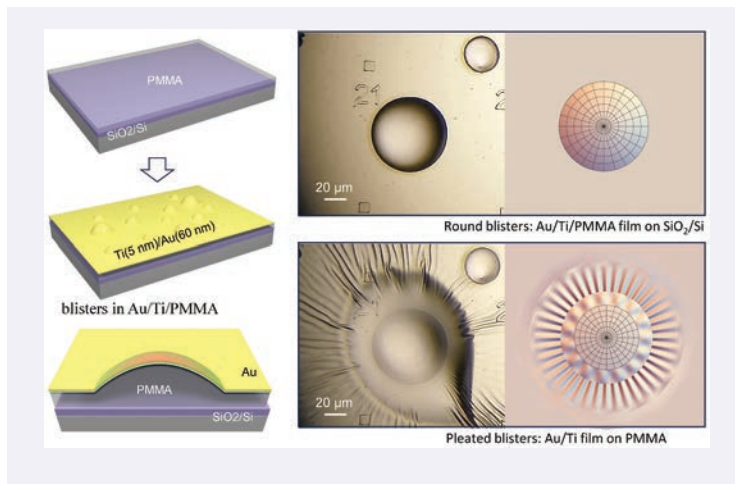
KEYWORDS

Electron beam deposition; heterojunctions; blisters; wrinkling; interface delamination

CONTACT Zhaohe Dai  daizh@pku.edu.cn  Department of Mechanics and Engineering Science, State Key Laboratory for Turbulence and Complex Systems, College of Engineering, Peking University, Beijing 100871, China

© 2025 The Author(s). Published by Informa UK Limited, trading as Taylor & Francis Group.

This is an Open Access article distributed under the terms of the Creative Commons Attribution-NonCommercial License (<http://creativecommons.org/licenses/by-nc/4.0/>), which permits unrestricted non-commercial use, distribution, and reproduction in any medium, provided the original work is properly cited. The terms on which this article has been published allow the posting of the Accepted Manuscript in a repository by the author(s) or with their consent.



1. Introduction

Thin-film deposition is a widely utilized process across various modern technologies, ranging from the semiconductor industry to the aerospace industry [1–3]. Electron beam deposition is a prominent thin-film fabrication technique offering high deposition rates (0.1–100 μm/min) at low substrate temperatures [4]. This method enables the production of high-purity, uniform metal films, making it particularly valuable for micro-electronic and optical applications where precision and material integrity are critical [5,6]. In a typical electron beam deposition process, a metal film is often deposited onto a substrate that has been pre-patterned with a thin polymethyl methacrylate (PMMA) layer, one of the first materials developed for electron beam lithography [6–8]. When deposition parameters, such as temperature and deposition rate [9], are not properly calibrated, gas blisters can form after the deposition of thin metal films, particularly with high atomic number target materials like Au and Ni [10–12].

The blistering phenomenon in electron beam evaporation of metallic thin films exhibits a dual nature. In micro-nano fabrication and precision manufacturing, it significantly compromises the accuracy of metallic patterns by distorting or damaging delicate features created during photolithographic processes [10]. Consequently, extensive trials and errors with fabrication parameters are often required to prevent blister formation [13–19]. Conversely, blister-induced structural alterations in thin films modify their crystalline architecture, enabling the regulation of electrical properties. Notably, tensile strain can reduce the bandgap of MoS₂ while enhancing carrier mobility, a strategic approach recognized as elastic strain engineering [20–23].

Although blister formation in thin films has been widely observed, most of them are focused on rigid substrates, such as Al₂O₃ on Si [15], graphene on hexagonal boron nitride (hBN) [24], there are few studies on the formation of blisters on substrates with deformability. The investigation of delamination and blistering dynamics in metallic thin films on flexible substrates is critical to advancing both fundamental interfacial mechanics and applied materials science. For thin films on rigid substrates, surface blistering is primarily attributed to two competing mechanisms: biaxial stress relaxation at the film-substrate

interface [25] and gas-induced pressure buildup during deposition processes [26]. Unlike rigid substrates, flexible systems introduce unique mechanical interactions, such as substrate compliance, which can significantly alter stress redistribution and gas entrapment dynamics. Furthermore, elucidating these mechanisms for metal thin film on flexible substrate not only bridges the gap between classical blistering theories and soft-material systems but also enables the development of predictive models for device durability – key to realizing robust, large-area flexible electronics for wearable technologies, biomedical devices, and adaptive optoelectronics [27].

Here, we investigate the formation mechanism of blisters that occur after depositing a Ti/Au film on a SiO_2/Si substrate coated with a spin-coated PMMA layer – an essential step in electronic device fabrication. Using elemental analysis and in situ heating experiments, we reveal that most blisters result from delamination between the Au-Ti-PMMA film and the SiO_2/Si substrate, typically exhibiting a relatively round shape. Additionally, a less common type of blister forms due to delamination between the Au-Ti film and the PMMA layer, characterized by radially wrinkled edges, which we term pleated blisters. We attribute the difference in blister morphology to variations in substrate deformability at the blister edge. Finally, we estimate the energy required to fracture the film-substrate interface and the typical strain levels within these blisters using a thin film mechanics model.

2. The blister geometry

We first briefly discuss the thin-film deposition process [28]. Figure 1(a) shows a schematic diagram of the electron beam deposition process, where the metal target and electron beam gun are positioned at the bottom, while the sample to be coated is placed at the top. When the electron beam bombards the metal target, the metal melts, and atoms overcome their cohesive energy, moving upward to deposit on the sample surface. The film thickness is monitored using a dedicated sensor. In Figure 1(b), we show the schematic diagram of blister

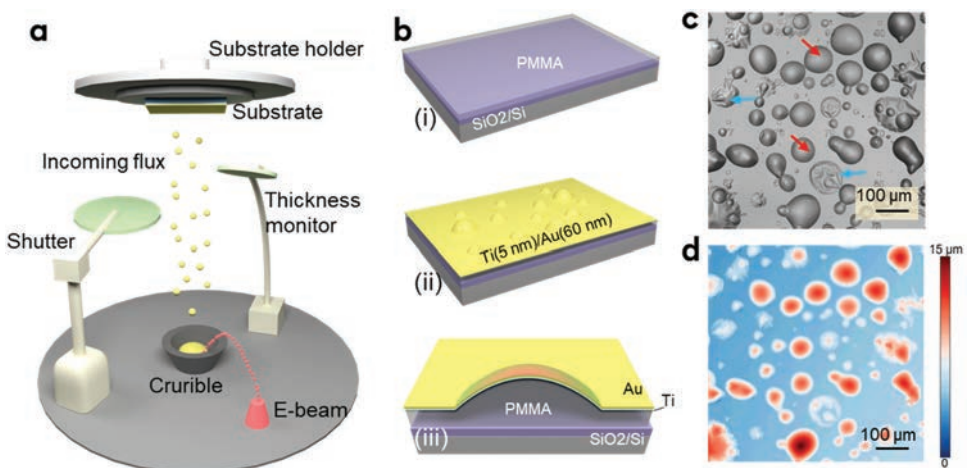


Figure 1. Blisters formed during electron beam evaporation. (a) Schematic of the electron beam evaporation setup. (b) Schematic of blister formation during the thin-film deposition process. (c,d) Optical and confocal microscope images of the fabricated thin films containing a number of blisters.

formation. Before depositing the film, the wafer substrate (P^{++} Si with 300 nm thermally grown SiO_2 obtained from Shanghai Onway Technology Co., Ltd.) underwent sequential ultrasonic cleaning in acetone, isopropyl alcohol (both purchased from Sigma-Aldrich), and deionized water for 15 minutes each. A 2% wt PMMA-950K solution (solvent: anisole) was then spin-coated onto the cleaned substrates at 3000 rpm for 60 s, followed by thermal annealing on a hot plate at 180°C for 2 minutes to remove solvent molecules from the film, forming a polymer layer approximately 300 nm thick (i). Ti and Au thin films were subsequently deposited using an electron beam evaporation system (E360) under an ultrahigh vacuum of 2×10^{-8} Pa, with deposition rates maintained between $0.5\text{--}2 \text{ \AA/s}$. A schematic and cross-sectional diagram of blister formation is shown at the bottom of Figure 1(b) (ii and iii) after the deposition of a thin composite metal film (a 5-nm-thick titanium adhesion layer and a 60-nm-thick Au layer). Figure 1(c,d) display optical and corresponding confocal microscope (LEXT OLS4000) images of the sample surface after electron beam deposition. Two distinct blister morphologies are evident. The more common type, which we term ‘round blisters,’ exhibits relatively circular shapes (indicated by red arrows in Figure 1(c)). The less common type, which we term ‘pleated blisters,’ displays wrinkled and often damaged geometries (indicated by blue arrows in Figure 1(c)). The diameters and heights of the round blisters, as measured in Figure 1(d), range from $36.7 \mu\text{m}$ to $129.1 \mu\text{m}$ and from $2.2 \mu\text{m}$ to $7.4 \mu\text{m}$, respectively. Due to their damaged geometry, accurate measurements of the pleated blisters are not feasible; however, it is evident that their horizontal dimensions are generally larger than those of the round blisters, while their heights are smaller. Wrinkled morphologies, a phenomenon absent in rigid substrates, such as blisters in Au/Si [16] and $Al_2O_3\text{--}ZnO/Si$ [12], can be attributed to the flexible PMMA layer, which is prone to Winkler-type deformation that causes wrinkling instabilities when the covering metal layer is in hoop compression.

Notably, when two round blisters are in close proximity, symmetry is disrupted even if they are separated by a short distance (Figure 2(a)). This observation suggests a ‘long-range interaction’ between the blisters, reminiscent of the classic ‘Cheerios effect’ observed in neighboring floating droplets [29–31]. The origin of this blister interaction should be attributed to the fact that the blister edges are not strictly clamped but are subject to certain slippage [32–34]. A direct consequence of this slippage toward the

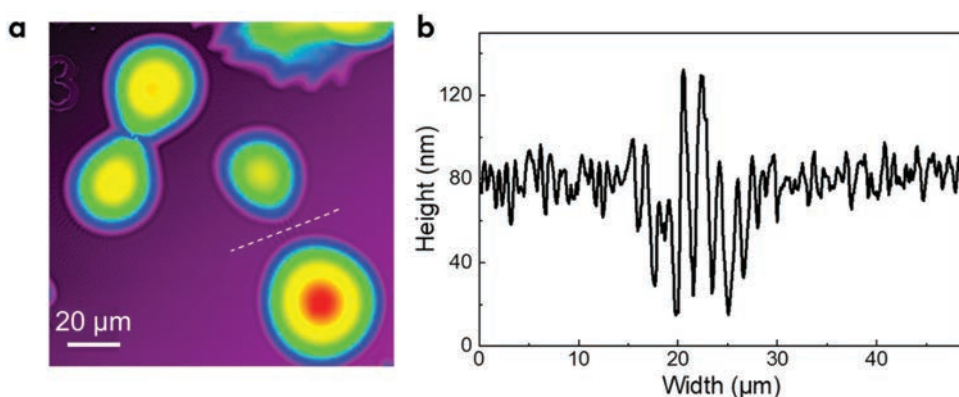


Figure 2. (a) Optical images of two adjacent round blisters. (b) The height profile measured along the white dashed line in (a).

blister is the occurrence of hoop compression near the blister edge, further leading to the formation of wrinkling instabilities [34–36] as verified by the profile measurement in Figure 2(b). The amplitude and wavelength of the wrinkles are approximately 100 nm and 1.6 μm , respectively. However, further interpretation of the wrinkled geometry is challenging due to the uncertainty regarding whether slippage occurs at the metal-PMMA interface or the PMMA-silicon interface.

The blistering behavior of the deposited thin films can persist in the fabrication of electronic devices, as demonstrated in the molybdenum disulfide (MoS_2 sheet obtained from Shanghai Onway Technology Co., Ltd.) based field-effect transistors (FET) [37]. We show the typical fabrication process in Figure 3(a). Firstly, a semiconductor MoS_2 sheet is first transferred onto a SiO_2/Si substrate (i). A layer of PMMA electron-beam resist is then spin-coated onto the substrate (ii). Electrode patterns are designed using L-edit software, followed by exposure of the PMMA layer to electron beams. After development and fixation, the PMMA is removed from the regions where electrodes are to be deposited (iii). The MoS_2 FET is then fabricated using the electron-beam evaporation of the thin metal film.

Figure 3(b) shows the morphology of a 5 nm titanium (Ti) adhesion layer and a 60 nm Au (Au) thin film deposited sequentially using electron beam deposition. Numerous blisters are observed in areas where the PMMA layer is present. In striking contrast, regions, where the PMMA layer has been removed during the fixation process (indicated by white arrows), appear relatively smooth and flat, suggesting that the observed blisters originate from the presence of the PMMA layer. This observation implies that the process of metal atoms with sufficient energy or high-energy particles, such as backscattered electrons, bombarding the PMMA layer, could cause residual solvent molecules in PMMA

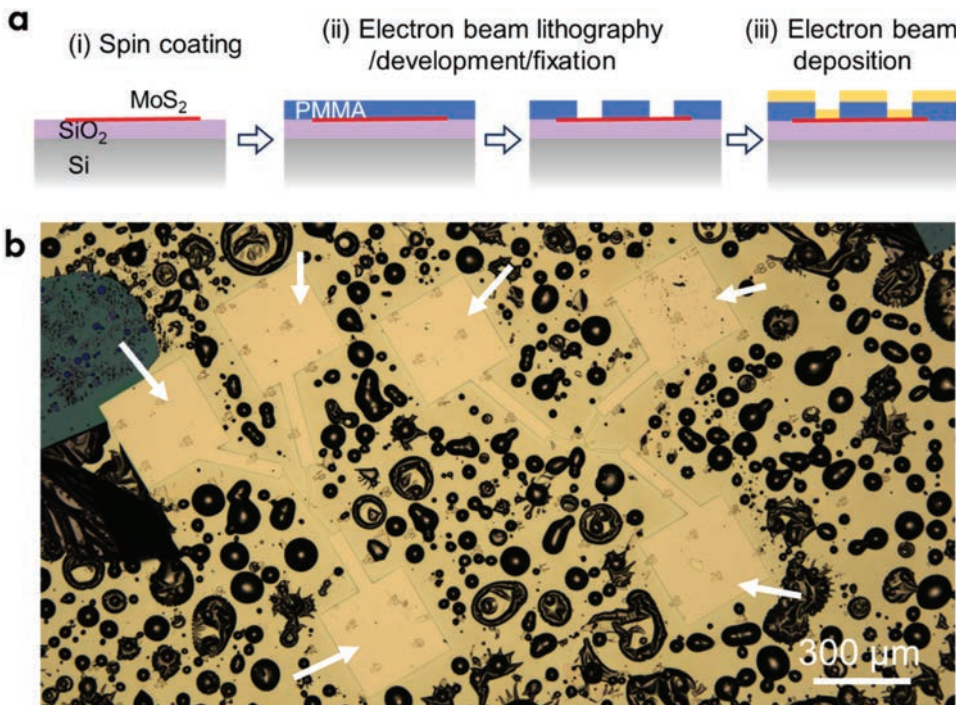


Figure 3. (a) Schematic illustration of the preparation process of MoS_2 -based micro-nano electronic devices. (b) Optical image of the device after depositing metal films.

to volatilize and aggregate at the Au-Ti/PMMA and PMMA/SiO₂ interface. The question remains, however: Which specific interface is responsible for the blistering? Answering this question is crucial for understanding the delamination mechanisms behind blister formation, which is key to controlling or suppressing the occurrence of blisters.

3. The delamination interfaces

It is intuitive to attribute the differences in the blister morphologies to two distinct film delamination interfaces: PMMA/SiO₂ and Au-Ti/PMMA. To test this hypothesis, we examine detailed ruptured films, which are typically associated with pleated blisters.

3.1. X-ray spectroscopy element analysis

In addition to blistering, the thin film in certain regions experiences fractures and inversion, as shown in [Figure 4\(a\)](#). After the initial (likely pleated) blister fractures, round blisters are also observed in the exposed area. This observation is consistent with that of the fractured and pleated blister seen in the top-left corner of [Figure 3\(b\)](#). This suggests that the fractured film is the metal layer delaminating from the PMMA, while the smaller round blisters correspond to the PMMA layer delaminating from the SiO₂ substrate. To verify, we perform the energy dispersive X-ray spectroscopy (EDS) element mapping of the surface utilizing a scanning electron microscope (SEM 4000Lv, 15 kV), as shown in [Figures 4b–f](#).

In the fractured blister, the exposed areas show a reduced presence of Ti and Au, with an increased presence of O, Si, and C elements. Since the C element originates from PMMA, elemental analysis suggests that delamination primarily occurs at the interface between the Au/Ti films and PMMA. Additionally, a small amount of PMMA is found to adhere to the metal thin film during the fracture and inversion process. In particular, the PMMA in the area indicated by the white arrow adhering to the SiO₂/Si substrate is also found in the area indicated by the red arrow ([Figure 4\(d\)](#)). The EDS experiment proves the existence of two delamination modes, both in the Au-Ti film on the PMMA layer and in the Au-Ti-PMMA film on the SiO₂ substrate.

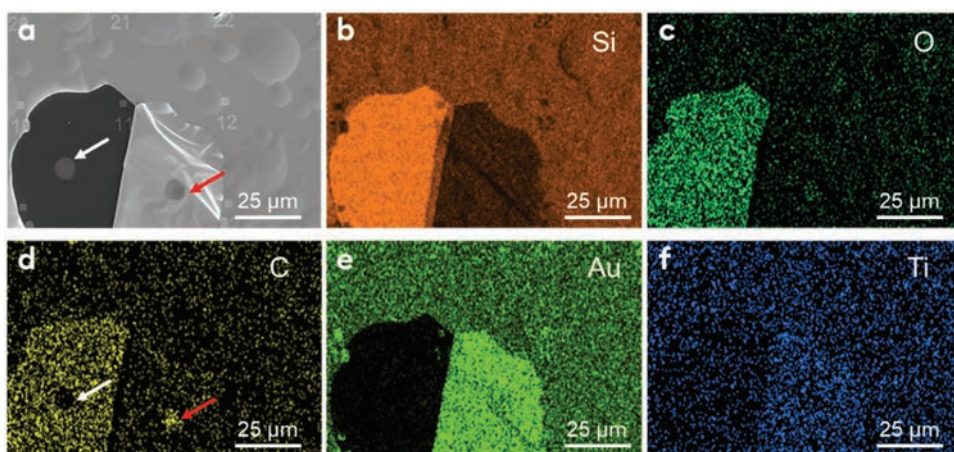


Figure 4. The energy dispersive X-ray spectroscopy element mapping of Au/Ti/PMMA on SiO₂/Si substrate.

3.2. In situ heating experiments

The formation of blisters during electron beam evaporation can be attributed to residual solvent molecules in the PMMA layer volatilizing and aggregating at either Au-Ti/PMMA or PMMA/SiO₂ interface. We then conduct in-situ heating experiments (EV300, heating rate: 2 °C/min) on the Au-Ti-PMMA-SiO₂-Si thin film system (Figure 5), carefully observing its morphological evolution as the temperature increases. We observe that below 50°C, the composite film maintains flat without the formation of discernible blisters. As the temperature reaches approximately 55°C, the film begins to wrinkle, indicating compressive stress on the metal layer [38,39]. This stress should be attributed to the mismatch in the coefficient of thermal expansion (CTE) between the metal layer and the polymer layers. Notably, the CTE values are $70\text{--}77 \times 10^{-6} \text{ K}^{-1}$ for PMMA, $8\text{--}15 \times 10^{-6} \text{ K}^{-1}$ for Au/Ti, and $0.5 \times 10^{-6} \text{ K}^{-1}$ for SiO₂ [40–42]. At 65°C, small blisters appear, accompanied by wrinkles, due to the release of solvent molecules from the PMMA layer. By the time the temperature reaches 75°C, the blisters have expanded significantly, yet they remain connected by regions of the film that have not fully delaminated. The blister formation is likely due to delamination between the metal film and the underlying PMMA layer. This delamination occurs because the thermal expansion mismatch between the two layers becomes too large to be compensated by the adhesive forces between them, causing the layers to separate and form blisters [43,44]. Interestingly, as the temperature gradually decreases, the blisters collapse and do not return to their initial state, suggesting that the blister formation process is largely irreversible. The collapse of the blisters indicates plastic deformation of the materials involved and permanent changes to the film structure due to thermal cycling.

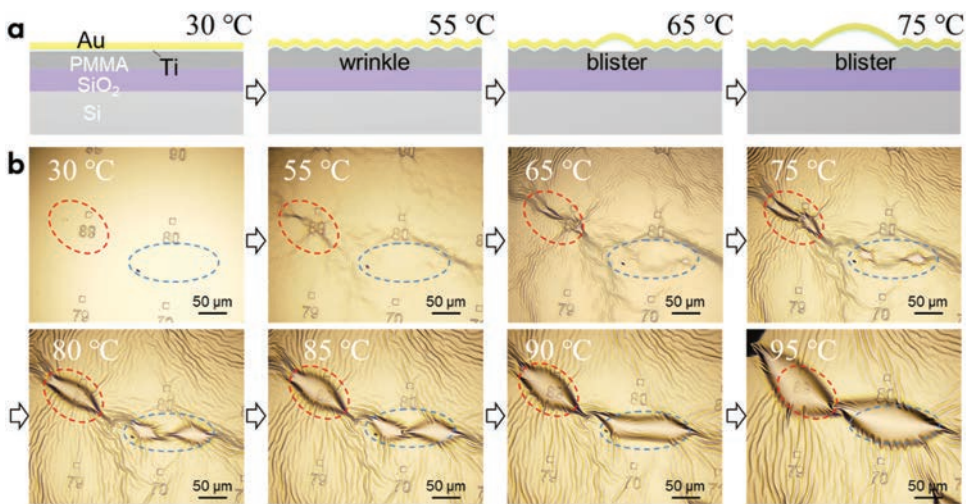


Figure 5. Delamination process in an initially flat area. Schematic diagram (a) and optical image (b) of evolution in blisters within an initially flat Au-Ti-PMMA with increasing temperature.

We then proceed to in-situ observation of heating an area initially containing round blisters (Figures 6a,b). Specifically, we focus on the morphological evolution of a 70 μm -diameter blister. Similarly, at around 55°C, wrinkles begin to form around the blister edge. As the temperature increases to 60°C, the outer edge of the wrinkled zone expands to approximately 30 μm , while the blister diameter remains unchanged. With further heating to 70°C, 80°C, and 90°C, the blister periphery exhibits radial delamination, leading to the formation of a new blister with increasing size. At 95°C, the edges of the initial blister (indicated by red arrows) become blurred due to the covering blister that is newly formed. These observations further confirm that the blisters formed during the in-situ heating experiments result from the delamination of the Au-Ti film from the PMMA layer. This also confirms that the initial round blister is indeed formed by the delamination of the entire Au-Ti-PMMA film from the SiO_2 substrate. Notably, unlike delamination from the rigid SiO_2 , the delamination of the metal film from the relatively soft polymer layer creates blisters with deformable edges, which are often accompanied by surrounding wrinkles near the blister edge.

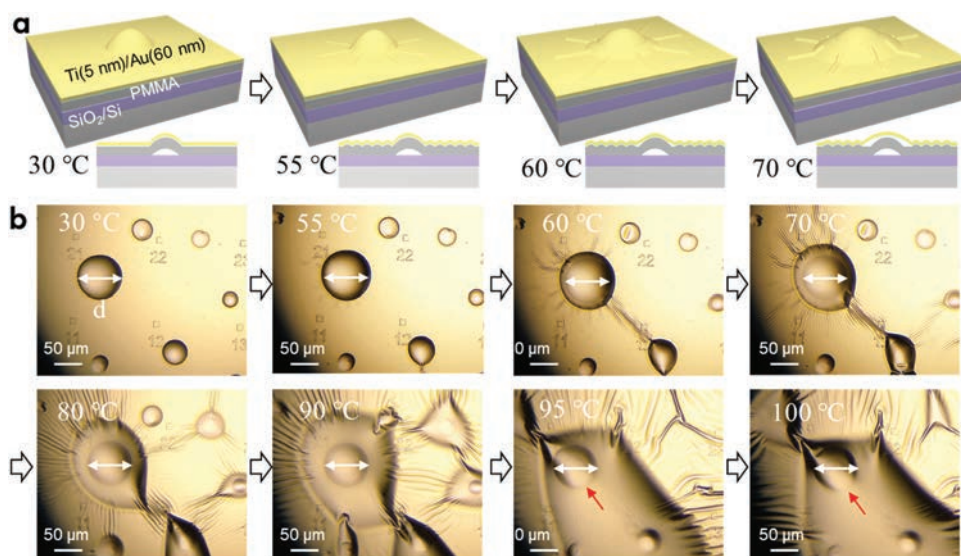


Figure 6. Heating an area that initially contained round blisters. (a) Schematic illustration of the evolution of the blister morphology upon heating. (b) Optical images showing the development of new blisters on top of the initially existing ones.

3.3. The formation mechanism

We have identified two types of blisters formed during the deposition of Ti/Au films on PMMA-coated SiO_2/Si substrates: Round blisters and pleated blisters (summarized in Figures 7a,b). Elemental analysis of pleated blisters and the in-situ heating experiments described above suggest that round blisters result from delamination of the Au-Ti-PMMA film from the SiO_2 substrate, while pleated blisters arise from delamination of the Au-Ti film and the substrate-supported PMMA layer. It can be hypothesized that when organic molecules in PMMA are thermally excited, they are

mostly trapped at the Au-Ti-PMMA/SiO₂ interface, leading to the formation of the commonly observed round blisters. In contrast, though less common, these molecules can accumulate at the Au-Ti/PMMA interface, leading to the formation of pleated blisters. The pleated geometry essentially arises from the deformable boundary at the blister edge, caused by the PMMA layer [45,46]. Such blisters with wrinkled geometries have been observed in similar but much smaller 2D crystal blisters [47], where the deformable boundary is provided by the van der Waals foundation at the crystal-substrate interface [36,48].

Importantly, the size and density of the blisters can be controlled by adjusting the deposition rate. As the deposition rate increased, the size and density of blisters decreased. In Figure 7(c), much fewer blisters are observed (with only round blisters and no pleated blisters) at a relatively fast deposition rate (Ti: 1 Å/s, Au: 2 Å/s). In Figure 7(d), there are a lot of blisters (including round and pleated) when the rates are halved (Ti: 0.5 Å/s, Au: 1 Å/s). The finding demonstrates that precise control of deposition kinetics enables the fabrication of defect-free thin films through optimized management of solvent dynamics. The cross-sectional view of the blister formation and non-blisters zone is shown in Figure 7(e). And SEM images of flat Au-Ti-PMMA film and Au-Ti-PMMA film with round blisters after in situ heating experiment are displayed in Figures 7f–g.

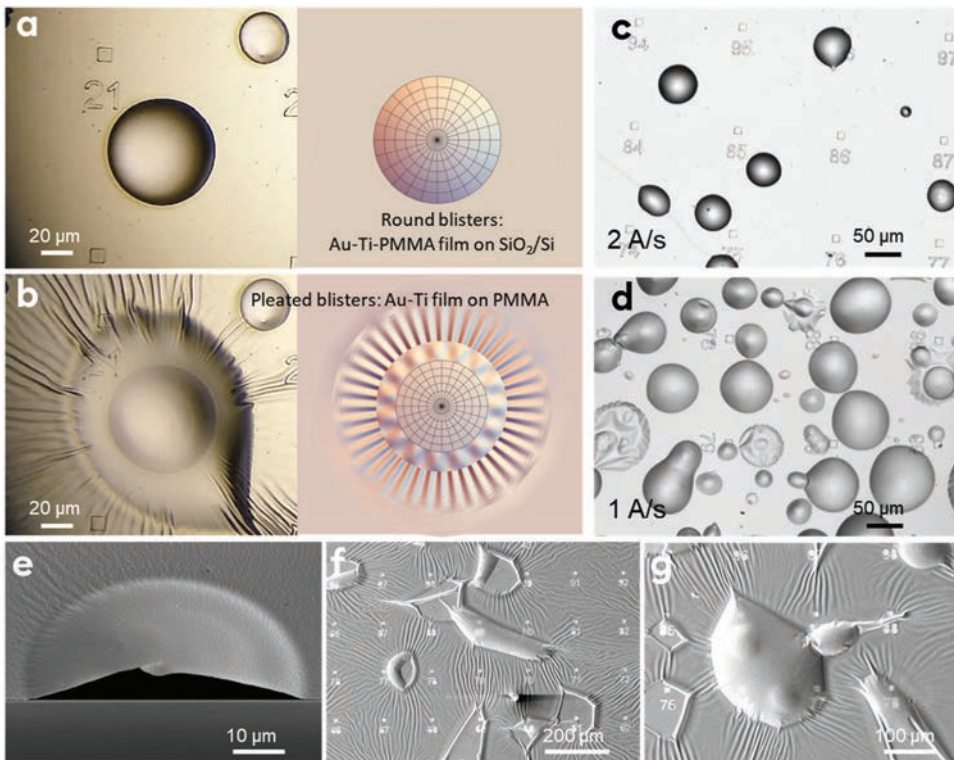


Figure 7. (a) Optical image of round blisters and their schematic illustration. (b) Optical image of a pleated blister and its schematic illustration. Morphology of blisters formed by depositing Au-Ti on PMMA at two different electron beam evaporation rates: 2 Å/s (c) and 1 Å/s (d). (e) SEM image of a round blister in the cross-sectional view. (f) SEM image of initially flat Au-Ti-PMMA film after in situ heating. (g) SEM image of Au-Ti-PMMA film initially with round blisters after in situ heating.

During film deposition, high-energy particle bombardment introduces compressive stress in the PMMA layer, while simultaneously generated heat triggers solvent volatilization. Although both compressive stress and solvent release could induce blisters, we observed an inverse correlation between blister size/density and deposition rate. Higher deposition rates (with elevated beam power and particle energy) paradoxically yield fewer blisters. This supports solvent volatilization coupled with the impermeable Au-Ti film as the dominant blistering mechanism. In addition, the thermal mismatch between PMMA and Au-Ti films primarily manifests in blister morphology. When delamination occurs at the Au-Ti-PMMA/SiO₂ interface, coordinated out-of-plane deformation of the Au-Ti-PMMA multilayer suppresses wrinkling, generating round blisters. Conversely, interfacial delamination between Au-Ti and PMMA accentuates thermal stress mismatch, leading to pleated blisters with pronounced surface wrinkling.

4. A thin-film mechanics model

Interfacial adhesion energy governs the delamination and blistering behavior of metal films, with higher adhesion energies corresponding to greater resistance against interfacial failure. Therefore, accurately determining the interfacial adhesion energy between thin films and substrates holds significant implications for interface engineering strategies. Nevertheless, quantifying adhesion energy becomes particularly challenging for nanoscale thin films due to experimental limitations in mechanical loading and pronounced interface interactions. Here, we show that the blister geometry can be directly used to indicate the interfacial adhesion energy, simply based on a thin-film mechanics model [49–51]. In addition, the out-of-plane geometry can be used to estimate the strain level in the thin film [52,53].

The blisters formed by the delamination of Ti-Au-PMMA from the SiO₂ substrate are commonly observed and relatively round, facilitating detailed measurements of their geometry. Figure 8(a) shows a 3D confocal profile of an area containing a bunch of round blisters. Here, we denote the blister height by h and the blister radius by a . Let r represent the radial distance from the blister center, and $w(r)$ denote the height profile. The height profiles of blisters of various sizes are extracted and summarized in Figure 8(b). We first attempt to analyze these profiles by fitting them with the function:

$$\frac{w(r)}{h} = \left(1 - \frac{r^2}{a^2}\right)^\alpha \quad (1)$$

where α is a fitting parameter that accounts for the specific geometry of the blister. Previous studies have shown that when bending effects dominate, the fitting parameter $\alpha = 2$, whereas in the membrane limit with negligible bending effects $\alpha \approx 1$ [24,54]. The solid curves in Figure 8(b) show a fit with $\alpha = 1$, confirming membrane-like deformation. This is not surprising since the blister height (in a few microns) has been much greater than the thickness of the relatively stiff metal film (~365 nm). A more accurate description can be performed via a perturbation analysis around this spherical cap shape [53].

In Figure 8(c), we plot the measured blister height as a function of the blister radius. A linear relationship is observed, with the height-to-radius ratio consistently around 0.19, independent of blister size. This suggests a steady-state interface delamination, as the characteristic length due to the interplay of the deformation of the metal and

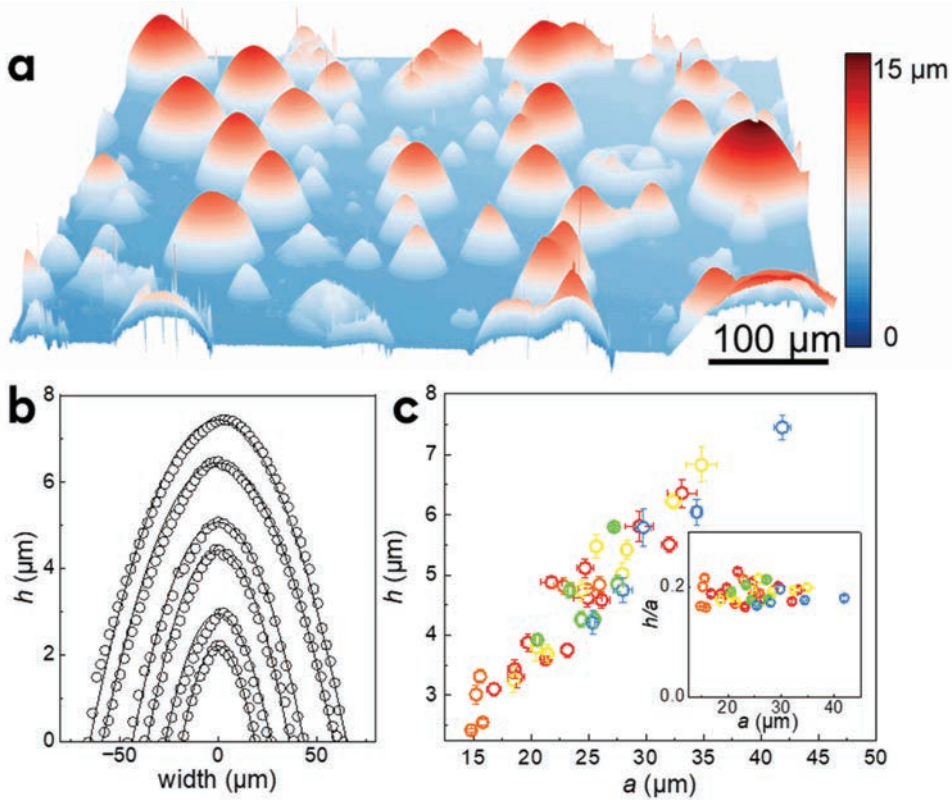


Figure 8. Interfacial blisters between Au-ti-PMMA film and SiO₂ substrate. (a) Three-dimensional profile of these blisters measured via a confocal microscope. (b) The height profile of typical blisters and its fitting by a parabolic function. (c) The relationship between the height h and radius a . The inset shows the relationship between the aspect ratio h/a and radius a .

polymer layers near the blister edge (~ 100 nm in Figure 2) is much smaller than the radius of the blisters (tens of microns) [55,56]. In this context, the interface toughness Γ between the Ti-Au-PMMA film and the SiO₂ substrate can be determined based on the thin-film blister model given in [57]:

$$\Gamma = \phi(\nu)Et \frac{h^4}{a^3} \quad (2)$$

where E is the Young's modulus of the composite film and $\phi(\nu)$ is a function of Poisson's ratio ν [53]. Particularly, an explicit expression for $\phi(\nu)$ has been discussed in [53] with accuracy comparable to the implicit Hencky's method:

$$\phi(\varepsilon, \nu) = \frac{5(7-\nu)}{24(1-\nu)} + \frac{5(53+\nu)}{126(1-\nu)} \varepsilon \quad (3)$$

where $\varepsilon \approx \frac{987-231\nu-7\sqrt{10985+3878\nu-3199\nu^2}}{12(139-67\nu)}$ results from the small correction due to the slight variation of the blister shape from the simple spherical cap shape. Since the film is an Au/Ti/PMMA composite layer, Young's modulus and Poisson's ratio are estimated by using the mixing principle. The Young's modulus of Au, Ti, and PMMA are 59–62 GPa [58–60], 100–120 GPa [61,62], and 2–4 GPa [63–65]. The Poisson ratios of Au, Ti, and PMMA are

approximately 0.41–0.44 [58,66], 0.32–0.36 [67,68], and 0.35–0.42 [69–71], respectively. Therefore, the effective modulus and the effective Poisson ratio are 12.7–15.1 GPa and 0.36–0.42. We can then estimate the interface toughness between the Ti-Au-PMMA film and SiO₂ substrate as around 41.7–53.7 J/m². While direct experimental data on Au-Ti-PMMA/SiO₂ multilayer systems remain limited in literature, previous blister test measurements under dry conditions have established adhesion energy values of 2.5–5 J/m² for PMMA/SiO₂ systems using axisymmetric loading configurations [72,73]. The reduced adhesion energy in our system originates from the rigid interlayer constraint imposed by the Au-Ti metallic film. This structural design restricts polymer deformation during delamination, significantly lowering the h/a ratio. Such constrained deformation modifies the energy dissipation pathway in the blister mechanics model, ultimately yielding lower calculated adhesion values. The primary limitation of this study lies in the current mechanical model, which assumes uniform thin-film deformation, whereas the Au-Ti-PMMA composite exhibits multilayered characteristics. Future efforts should focus on developing advanced constitutive models to better capture the mechanical behavior of multilayer composite film systems. Similarly, we can also estimate the strain levels in the composite film, which have been given in terms of radial and hoop strain distributions [53]:

$$\varepsilon_{rr} = \left(\frac{h}{a}\right)^2 \frac{f(\varepsilon, \nu) - 56(1-3\nu)R^2 - 64(1-6\nu)R^5\varepsilon - 35(1-9\nu)R^8\varepsilon^2}{224(1+\varepsilon)^2} \quad (4)$$

and

$$\varepsilon_{\theta\theta} = \left(\frac{h}{a}\right)^2 \frac{f(\varepsilon, \nu) - 56(3-\nu)R^2 - 64(6-\nu)R^5\varepsilon - 35(9-\nu)R^8\varepsilon^2}{224(1+\varepsilon)^2} \quad (5)$$

where $f(\varepsilon, \nu) = 56(3 - \nu) + 64(6 - \nu)\varepsilon + 35(9 - \nu)\varepsilon^2$, R is r/a . Plugging $h/a \approx 0.19$, we find the equal-biaxial strain level at the blister center ($r = 0$) is around 2.26%, which is considerably large for strain engineering applications of typical semiconductor films [22].

4. Conclusions

In summary, we have discussed the formation of blisters when depositing Au-Ti film on PMMA layers. We have shown that the number and size of these blisters could decrease with the increase in deposition rate. *In situ* observations were conducted to examine the morphological evolution of both flat and pre-blistered Au-Ti-PMMA films as a function of temperature. Due to thermal mismatch between the Au-Ti film and substrate-supported PMMA layer, complex wrinkling patterns occurred in both types of films at 55°C. For pre-blistered Au-Ti-PMMA films, delamination propagated outward along the edges of the preexisting blisters, which indicates that two delamination interfaces in the formed blisters. We have revealed that blisters with round geometries are formed by the delamination of the Au-Ti-PMMA film from the SiO₂ substrate, while blisters with complex wrinkled, pleated geometries arise from the delamination of the Au-Ti film from the PMMA layer. For the deposition-induced blisters, we extracted height profiles using 3D confocal microscopy, showing a characteristic height-to-radius ratio. This ratio helps to reveal the interface toughness between the Au-Ti-PMMA film and the substrate, as well as the typical strain levels in the film.

Disclosure statement

No potential conflict of interest was reported by the author(s).

Funding

This work was financially supported by the National Natural Science Foundation of China [Grant No. 12372103 and 12432003].

References

- [1] Hoffmann W, Pellkofer T. Thin films in photovoltaics: technologies and perspectives. *Thin Solid Films*. 2012;520(12):4094–4100. doi: [10.1016/j.tsf.2011.04.146](https://doi.org/10.1016/j.tsf.2011.04.146)
- [2] Xie G, Bai H, Miao G, et al. The applications of ultra-thin nanofilm for aerospace advanced manufacturing technology. *Nanomaterials*. 2021;11(12):3282. doi: [10.3390/nano11123282](https://doi.org/10.3390/nano11123282)
- [3] Gupta SK, Jha P, Singh A, et al. Flexible organic semiconductor thin films. *J Mater Chem C*. 2015;3(33):8468–8479. doi: [10.1039/C5TC00901D](https://doi.org/10.1039/C5TC00901D)
- [4] Eessaa AK, El-Shamy AM. Review on fabrication, characterization, and applications of porous anodic aluminum oxide films with tunable pore sizes for emerging technologies. *Microelectron Eng*. 2023;279:112061. doi: [10.1016/j.mee.2023.112061](https://doi.org/10.1016/j.mee.2023.112061)
- [5] Chen S, Jin J, Wang W, et al. Thermally tunable anti-ambipolar heterojunction devices. *hys Chem Chem Phys*. 2024;26(35):23438. doi: [10.1039/D4CP02937B](https://doi.org/10.1039/D4CP02937B)
- [6] Wang W, Jin J, Wang Y, et al. High-speed optoelectronic nonvolatile memory based on van der Waals heterostructures. *Small*. 2023;19(47):e2304730. doi: [10.1002/sml.202304730](https://doi.org/10.1002/sml.202304730)
- [7] Tseng AA, Kuan C, Chen CD, et al. Electron beam lithography in nanoscale fabrication: recent development. *IEEE Trans Electron Packag Manufact*. 2003;26(2):141–149. doi: [10.1109/TEPM.2003.817714](https://doi.org/10.1109/TEPM.2003.817714)
- [8] Doh YJ, van Dam JA, Roest AL, et al. Tunable supercurrent through semiconductor nanowires. *Science*. 2005;309(5732):272–275. doi: [10.1126/science.1113523](https://doi.org/10.1126/science.1113523)
- [9] Wu CY, Chen JH, Kuo CG, et al. Effects of deposition parameters on the structure and properties of ZrN, WN and ZrWN films. *Bull Mater Sci*. 2019;42(1):38. doi: [10.1007/s12034-018-1719-7](https://doi.org/10.1007/s12034-018-1719-7)
- [10] Sun B, Grap T, Frahm T, et al. Role of electron and ion irradiation in a reliable lift-off process with electron beam evaporation and a bilayer PMMA resist system. *J Vac Sci Technol B*. 2021;39(5):052601. doi: [10.1116/6.0001161](https://doi.org/10.1116/6.0001161)
- [11] Bras P, Sterner J, Platzer-Björkman C. Investigation of blister formation in sputtered Cu₂ZnSnS₄ absorbers for thin film solar cells. *J Vac Sci Technol A*. 2015;33(6):061201. doi: [10.1116/1.4926754](https://doi.org/10.1116/1.4926754)
- [12] Liu H, Guo S, Yang RB, et al. Giant blistering of nanometer-thick Al₂O₃/ZnO films grown by atomic layer deposition: mechanism and potential applications. *ACS Appl Mater Interfaces*. 2017;9(31):26201–26209. doi: [10.1021/acsami.7b08260](https://doi.org/10.1021/acsami.7b08260)
- [13] Pandey M, Ahuja R, Kumar R. Viscous fingering instabilities in spontaneously formed blisters of MoS₂ multilayers. *Nanoscale Adv*. 2023;5(23):6617–6625. doi: [10.1039/D3NA00563A](https://doi.org/10.1039/D3NA00563A)
- [14] Malerba C, Valentini M, Azanza Ricardo CL, et al. Blistering in Cu₂ZnSnS₄ thin films: correlation with residual stresses. *Mater Design*. 2016;108:725–735. doi: [10.1016/j.matdes.2016.07.019](https://doi.org/10.1016/j.matdes.2016.07.019)
- [15] Zhao S, Yuan G, Zhang D, et al. Formation and elimination mechanism of thermal blistering in Al₂O₃/Si system. *J Mater Sci*. 2021;56(31):17478–17489. doi: [10.1007/s10853-021-06441-9](https://doi.org/10.1007/s10853-021-06441-9)
- [16] Cao J, Yuan B, Gong N, et al. Insights into thin film blistering of gold coating on metal substrate. *Appl Surf Sci*. 2023;611:155700. doi: [10.1016/j.apsusc.2022.155700](https://doi.org/10.1016/j.apsusc.2022.155700)
- [17] Webb E, Witt C, Andryuschenko T, et al. Integration of thin electroless copper films in copper interconnect metallization. *J Appl Electrochem*. 2004;34(3):291–300. doi: [10.1023/B:JACH.0000015618.02583.f7](https://doi.org/10.1023/B:JACH.0000015618.02583.f7)

- [18] Blanchard-Dionne A-P, Meunier M. Electron beam lithography using a PMMA/P(MMA 8.5 MAA) bilayer for negative tone lift-off process. *J Vac Sci Technol B*. 2015;33(6):061602. doi: [10.1116/1.4935129](#)
- [19] Volmer F, Seidler I, Bisswanger T, et al. How to solve problems in micro- and nanofabrication caused by the emission of electrons and charged metal atoms during e-beam evaporation. *J Phys D: Appl Phys*. 2021;54(22):225304. doi: [10.1088/1361-6463/abe89b](#) Polymer curing assisted formation of optically visible sub-micron blisters of multilayer graphene for local strain engineering
- [20] Pandey M, Kumar R. Polymer curing assisted formation of optically visible sub-micron blisters of multilayer graphene for local strain engineering. *J Phys: Condens Matter*. 2022;34(24):245401. doi: [10.1088/1361-648X/ac61b4](#)
- [21] Levy N, Burke SA, Meaker KL, et al. Strain-induced pseudo-magnetic fields greater than 300 tesla in graphene nanobubbles. *Science*. 2010;329(5991):544–547. doi: [10.1126/science.1191700](#)
- [22] Kang S, Jeon S, Kim S, et al. Tunable out-of-plane piezoelectricity in thin-layered MoTe2 by surface corrugation-mediated flexoelectricity. *ACS Appl Mater Interfaces*. 2018;10(32):27424–27431. doi: [10.1021/acsami.8b06325](#)
- [23] Dai Z, Liu L, Zhang Z. Strain engineering of 2D materials: issues and opportunities at the interface. *Adv Mater*. 2019;31(45):e1805417. doi: [10.1002/adma.201805417](#)
- [24] Wang W, Ma X, Dai Z, et al. Mechanical behavior of blisters spontaneously formed by multilayer 2D materials. *Adv Mater Interface*. 2022;9(12):2101939. doi: [10.1002/admi.202101939](#)
- [25] Yang ZX, He XT, Wen SR. Closed-form solution and experimental verification for the axisymmetric deformation problem of blistering circular thin polymer films under uniformly distributed gas pressure. *Polymers*. 2020;12(5):1130. doi: [10.3390/polym12051130](#)
- [26] van den Bos RAJM, Reinink J, Lopaev DV, et al. Influence of internal stress and layer thickness on the formation of hydrogen induced thin film blisters in Mo/Si multilayers. *J Phys D: Appl Phys*. 2018;51(11):115302. doi: [10.1088/1361-6463/aaad86](#)
- [27] Cheng T, Zhang Y, Lai WY, et al. Stretchable thin-film electrodes for flexible electronics with high deformability and Stretchability. *Adv Mater*. 2015;27(22):3349–3376. doi: [10.1002/adma.201405864](#)
- [28] Wnuk JD, Rosenberg SG, Gorham JM, et al. Electron beam deposition for nanofabrication: insights from surface science. *Surf Sci*. 2011;605(3–4):257–266. doi: [10.1016/j.susc.2010.10.035](#)
- [29] Vella D, Mahadevan L. The “cheerios effect. *Am J Phys*. 2005;73:817–825.
- [30] Karpitschka S, Pandey A, Lubbers LA, et al. Liquid drops attract or repel by the inverted cheerios effect. *Proc Natl Acad Sci USA*. 2016;113(27):7403–7407. doi: [10.1073/pnas.1601411113](#)
- [31] Dai Z, Vella D. Droplets on lubricated surfaces: the slow dynamics of skirt formation. *Phys Rev Fluids*. 2022;7(5):054003. doi: [10.1103/PhysRevFluids.7.054003](#)
- [32] Dai Z, Lu N. Poking and bulging of suspended thin sheets: slippage, instabilities, and metrology. *J Mech Phys Solids*. 2021;149:104320. doi: [10.1016/j.jmps.2021.104320](#)
- [33] Dai Z, Lu N, Liechti KM, et al. Mechanics at the interfaces of 2D materials: challenges and opportunities. *Curr Opin Solid State Mater Sci*. 2020;24(4):100837. doi: [10.1016/j.cossms.2020.100837](#)
- [34] Dai Z, Sanchez DA, Brennan CJ, et al. Radial buckle delamination around 2D material tents. *J Mech Phys Solids*. 2020;137:103843. doi: [10.1016/j.jmps.2019.103843](#)
- [35] Davidovitch B, Guinea F. Indentation of solid membranes on rigid substrates with van der Waals attraction. *Phys Rev E*. 2021;103(4):043002. doi: [10.1103/PhysRevE.103.043002](#)
- [36] Ares P, Wang YB, Woods CR, et al. Van der Waals interaction affects wrinkle formation in two-dimensional materials. *Proc Natl Acad Sci USA*. 2021;118(14):e2025870118. doi: [10.1073/pnas.2025870118](#)
- [37] Wang W, Wei Z, Li YJ, et al. Multifunctional complementary field-effect transistors based on MoS₂/SWNTs heterostructures. *Appl Phys Lett*. 2025;126(2):0245016. doi: [10.1063/5.0245016](#)
- [38] Liu S, He J, Rao Y, et al. Conformability of flexible sheets on spherical surfaces. *Sci Adv*. 2023;9(16):eadf2709. doi: [10.1126/sciadv.adf2709](#)

- [39] Box F, Domino L, Corvo TO, et al. Delamination from an adhesive sphere: curvature-induced dewetting versus buckling. *Proc Natl Acad Sci USA*. 2023;120(12):e2212290120. doi: [10.1073/pnas.2212290120](https://doi.org/10.1073/pnas.2212290120)
- [40] Cariou JM, Dugas J, Martin L, et al. Refractive-index variations with temperature of PMMA and polycarbonate. *Appl Opt*. 1986;25(3):334–336. doi: [10.1364/AO.25.000334](https://doi.org/10.1364/AO.25.000334)
- [41] Zhan T, Wang H, Xu Y. Unexpectedly high thermal boundary resistance of Cr/graphene/SiO₂ structure. *Jpn J Appl Phys*. 2017;56(5):055101. doi: [10.7567/JJAP.56.055101](https://doi.org/10.7567/JJAP.56.055101)
- [42] Elomari S, Skibo MD, Sundararajan A, et al. Thermal expansion behavior of particulate metal-matrix composites. *Compo Sci Technol*. 1998;58(3–4):369–376. doi: [10.1016/S0266-3538\(97\)00124-3](https://doi.org/10.1016/S0266-3538(97)00124-3)
- [43] Mei H, Landis CM, Huang R. Concomitant wrinkling and buckle-delamination of elastic thin films on compliant substrates. *Mech Mater*. 2011;43(11):627–642. doi: [10.1016/j.mechmat.2011.08.003](https://doi.org/10.1016/j.mechmat.2011.08.003)
- [44] Pan K, Ni Y, He L, et al. Nonlinear analysis of compressed elastic thin films on elastic substrates: from wrinkling to buckle-delamination. *Int J Mech Sci*. 2014;51(21–22):3715–3726. doi: [10.1016/j.ijsolstr.2014.07.005](https://doi.org/10.1016/j.ijsolstr.2014.07.005)
- [45] Li J, Zhang G, Wang L, et al. Indentation of a plate on a thin transversely isotropic elastic layer. *Acta Mech Solida Sin*. 2024;38(2):331–340. doi: [10.1007/s10338-024-00532-1](https://doi.org/10.1007/s10338-024-00532-1)
- [46] Yu C, Dai Z. Premature jump-to-contact with elastic surfaces. *J Mech Phys Solids*. 2024;193:105919. doi: [10.1016/j.jmps.2024.105919](https://doi.org/10.1016/j.jmps.2024.105919)
- [47] Yu C, Cao J, Zhu S, et al. Preparation and modeling of graphene bubbles to obtain strain-induced pseudomagnetic fields. *Materials*. 2024;17(12):2889. doi: [10.3390/ma17122889](https://doi.org/10.3390/ma17122889)
- [48] Dai Z, Rao Y, Lu N. Two-dimensional crystals on adhesive substrates subjected to uniform transverse pressure. *Int J Mech Sci*. 2022;257:111829. doi: [10.1016/j.ijsolstr.2022.111829](https://doi.org/10.1016/j.ijsolstr.2022.111829)
- [49] Fang Z, Dai Z, Wang B, et al. Pull-to-peel of two-dimensional materials for the simultaneous determination of elasticity and adhesion. *Nano Lett*. 2023;23(2):742–749. doi: [10.1021/acs.nanolett.2c03145](https://doi.org/10.1021/acs.nanolett.2c03145)
- [50] Chen E, Dai Z. Axisymmetric peeling of thin elastic films: a perturbation solution. *J Appl Mech*. 2023;90(10):101011. doi: [10.1115/1.4062831](https://doi.org/10.1115/1.4062831)
- [51] Afferrante L, Carbone G, Demelio G, et al. Adhesion of elastic thin films: double peeling of tapes versus axisymmetric peeling of membranes. *Tribol Lett*. 2013;52(3):439–447. doi: [10.1007/s11249-013-0227-6](https://doi.org/10.1007/s11249-013-0227-6)
- [52] Dai Z, Hou Y, Sanchez DA, et al. Interface-governed deformation of nanobubbles and nanotents formed by two-dimensional materials. *Phys Rev Lett*. 2018;121(26):266101. doi: [10.1103/PhysRevLett.121.266101](https://doi.org/10.1103/PhysRevLett.121.266101)
- [53] Dai Z. Analytical solutions for circular elastic membranes under pressure. *J Appl Mech*. 2024;91(8):081002. doi: [10.1115/1.4065338](https://doi.org/10.1115/1.4065338)
- [54] Wang G, Dai Z, Xiao J, et al. Bending of multilayer van der Waals materials. *Phys Rev Lett*. 2019;123(11):116101. doi: [10.1103/PhysRevLett.123.116101](https://doi.org/10.1103/PhysRevLett.123.116101)
- [55] Li H, Dai Z. Adhesion of elastic microbeams on thin deformable substrates. *Eng Fract Mech*. 2025;313:110634. doi: [10.1016/j.engfracmech.2024.110634](https://doi.org/10.1016/j.engfracmech.2024.110634)
- [56] Li H, Yu C, Dai Z. Regimes in the axisymmetric stiction of thin elastic plates. *Int J Mech Sci*. 2024;284:109740. doi: [10.1016/j.ijmecsci.2024.109740](https://doi.org/10.1016/j.ijmecsci.2024.109740)
- [57] Sanchez DA, Dai Z, Wang P, et al. Mechanics of spontaneously formed nanoblisters trapped by transferred 2D crystals. *Proc Natl Acad Sci USA*. 2018;115(31):7884. doi: [10.1073/pnas.1801551115](https://doi.org/10.1073/pnas.1801551115)
- [58] Lee SJ, Han SW, Hyun SM, et al. Measurement of Young's modulus and Poisson's ratio for thin Au films using a visual image tracing system. *Curr Appl Phys*. 2009;9(1):S75–S78. doi: [10.1016/j.cap.2008.08.048](https://doi.org/10.1016/j.cap.2008.08.048)
- [59] Wang J, Qin H, Chen J, et al. First-principles study on the elastic mechanical properties and anisotropies of gold–copper intermetallic compounds. *Metals*. 2022;12(6):959. doi: [10.3390/met12060959](https://doi.org/10.3390/met12060959)
- [60] Kikuchi M, Takahashi M, Okuno O. Elastic moduli of cast Ti–Au, Ti–Ag, and Ti–Cu alloys. *Dent Mater*. 2006;22(7):641–646. doi: [10.1016/j.dental.2005.05.015](https://doi.org/10.1016/j.dental.2005.05.015)

- [61] Lutfullin RY, Trofimov EA, Kashaev RM, et al. Young's modulus of titanium alloy VT₆S and its structural sensitivity. *Mater Lett.* **2017**;7(1):12–16. doi: [10.22226/2410-3535-2017-1-12-16](https://doi.org/10.22226/2410-3535-2017-1-12-16)
- [62] Marker C, Shang S-L, Zhao J-C, et al. Effects of alloying elements on the elastic properties of bcc Ti-X alloys from first-principles calculations. *Comp Mater Sci.* **2018**;142:215–226. doi: [10.1016/j.commatsci.2017.10.016](https://doi.org/10.1016/j.commatsci.2017.10.016)
- [63] Lopez A, Hoess A, Thersleff T, et al. Low-modulus PMMA bone cement modified with castor oil. *Biomed Mater Eng.* **2011**;21(5–6):323–332. doi: [10.3233/BME-2012-0679](https://doi.org/10.3233/BME-2012-0679)
- [64] Zhi CY, Bando Y, Wang WL, et al. Mechanical and thermal properties of polymethyl Methacrylate-BN nanotube composites. *J Nanomater.* **2008**;2008(1):5. doi: [10.1155/2008/642036](https://doi.org/10.1155/2008/642036)
- [65] Abdel-Wahab AA, Ataya S, Silberschmidt VV. Temperature-dependent mechanical behaviour of PMMA: experimental analysis and modelling. *Polym Test.* **2017**;58:86–95. doi: [10.1016/j.polymertesting.2016.12.016](https://doi.org/10.1016/j.polymertesting.2016.12.016)
- [66] Oliva AI, Comparán-Rodríguez GG, Sosa V, et al. Poisson's ratio determination of Au nanofilms by piezoresistive measurements. *J Mater Sci.* **2023**;58(20):8563–8571. doi: [10.1007/s10853-023-08536-x](https://doi.org/10.1007/s10853-023-08536-x)
- [67] Hao YL, Li SJ, Sun BB, et al. Ductile titanium alloy with low Poisson's ratio. *Phys Rev Lett.* **2007**;98(21):216405. doi: [10.1103/PhysRevLett.98.216405](https://doi.org/10.1103/PhysRevLett.98.216405)
- [68] Greaves GN, Greer AL, Lakes RS, et al. Poisson's ratio and modern materials. *Nat Mater.* **2011**;10(11):823–837. doi: [10.1038/nmat3134](https://doi.org/10.1038/nmat3134)
- [69] Li Y, Wang L, Jiang H. Solving poisson's ratio of single-layer composites acted by normal force with interface non-slip condition. *IOP Conf Ser: Earth Environ Sci.* **2019**;310(4):042001. doi: [10.1088/1755-1315/310/4/042001](https://doi.org/10.1088/1755-1315/310/4/042001)
- [70] Nguyen C, Maheshwari V, Saraf RF. Ultrasoft 100 nm thick zero Poisson's ratio film with 60% reversible compressibility. *Nano Lett.* **2012**;12(4):2171–2175. doi: [10.1021/nl300686c](https://doi.org/10.1021/nl300686c)
- [71] Cuddalorepatta GK, van Rees WM, Han L, et al. Poisson's ratio and residual strain of free-standing ultra-thin films. *J Mech Phys Solids.* **2020**;137:103821. doi: [10.1016/j.jmps.2019.103821](https://doi.org/10.1016/j.jmps.2019.103821)
- [72] Cui L, Ranade AN, Matos MA, et al. Improved adhesion of dense silica coatings on polymers by atmospheric plasma pretreatment. *ACS Appl Mater Interfaces.* **2013**;5(17):8495–8504. doi: [10.1021/am401921k](https://doi.org/10.1021/am401921k)
- [73] Tan KT, White CC, Hunston DL, et al. Fundamentals of adhesion failure for a model adhesive (PMMA/Glass) joint in humid environments. *J Adhes.* **2008**;84(4):339–367. doi: [10.1080/00218460802004428](https://doi.org/10.1080/00218460802004428)